Atomic Layer Deposition of SiO_2 and TiO_2 in Alumina Tubular Membranes: Pore Reduction and Effect of Surface Species on Gas Transport

M. A. Cameron, I. P. Gartland,† J. A. Smith, S. F. Diaz,‡ and S. M. George*

Department of Chemistry and Biochemistry, University of Colorado, Boulder, Colorado 80309

Received December 31, 1999. In Final Form: April 7, 2000

The pore diameters in alumina tubular membranes were progressively reduced via SiO_2 and TiO_2 atomic layer deposition (ALD) using sequential surface reactions. The SiO_2 ALD was accomplished using alternating exposures of $SiCl_4$ and H_2O. The TiO_2 ALD was achieved using alternating exposures of $TiCl_4$ and H_2O. The reduction of the pore diameter was observed using in situ N_2 conductance measurements. The total conductance, $C_t = Q/\Delta P_t$, was measured using a mass flow controller to define a constant gas throughput, Q, and two capacitance manometers to monitor the total pressure drop, ΔP_t. These N_2 conductance measurements revealed that the SiO_2 and TiO_2 ALD progressively reduced the pore diameter from an initial diameter of 50 Å to molecular diameters. Using an aperture model for the conductance, the pore diameter was found to decrease at a rate of 1.3 ± 0.1 Å per $SiCl_4/H_2O$ AB cycle during SiO_2 deposition and 3.1 ± 0.9 Å per $TiCl_4/H_2O$ AB cycle during TiO_2 deposition. The N_2 conductance measurements were also very sensitive to the functional groups on the surface of the pores. The $SiCl_4$ and $TiCl_4$ exposures leave the pore surface terminated with SiCl* and TiCl* surface species, respectively. Subsequent exposure to H_2O converts these surface species to SiOH* or TiOH* species. During SiO_2 deposition, the pore diameters are 0.9 ± 0.2 Å larger after the H_2O exposure replaces the SiCl* species with the SiOH* species. During TiO_2 deposition, the pore diameters are 0.7 ± 0.2 Å larger after the H_2O exposure replaces the TiCl* species with the TiOH* species. These pore diameter differences are somewhat smaller than the differences predicted by steric interaction calculations of bond lengths and van der Waals hard sphere radii for these surface functional groups. The N_2 conductance measurements illustrate that gas transport through microscopic pores is determined by pore diameters and the effect of the surface species.

I. Introduction

Porous inorganic membranes are useful because of their mechanical, chemical, and thermal stability. These properties enable porous inorganic membranes to be employed for gas separations at high temperatures under corrosive conditions.[1−3] One limitation on the application of current porous inorganic membranes is their relatively large minimum pore diameter of ≥30−50 Å.[4,5] At these pore diameters, gas transport is controlled primarily by Knudsen diffusion or capillary condensation mechanisms.[6,7] Much more efficient separation could be achieved if the pore diameters were reduced to molecular dimensions. In this regime, molecular sieving interactions and surface interactions become dominant and may offer enhanced gas selectivity.[8−10]

Pore diameters in inorganic membranes can be reduced using a variety of chemical vapor deposition (CVD) methods. Chemical vapor infiltration methods can be employed using either single or multiple gas precursors.[11−13] For the location of the deposition within the porous membrane to be controlled, the precursors for a binary CVD reaction can be introduced on opposite sides of the membrane using the opposing reactant geometry.[5,14,15] Higher control of the thickness and uniformity of the deposition on the pores can be obtained using sequential, alternating exposures of the two reactants.[16−20] This modified CVD method is also referred to as atomic layer epitaxy (ALE) or atomic layer deposition (ALD).[21]

We have demonstrated earlier that pore diameters in inorganic membranes can be reduced to molecular dimensions using the ALD method.[17−19] Pore reduction occurred using alternating exposures of $Al(CH_3)_3$ and H_2O

* Corresponding author. Telephone: (303) 492-3398. Fax: (303) 492-5894. E-mail: GeorgeS@Spot.Colorado.Edu

† Present address: Eltron Research Inc., 5660 Airport Blvd., Boulder, CO 80301.

‡ Present address: Department of Chemistry, University of Washington, Seattle, WA 98195.

(1) Hseih, H. P. *Inorganic Membranes for Separation and Reaction*, 3rd ed.; Elsevier: New York, 1996.

(2) Bhave, R. R. *Inorganic Membranes Synthesis, Characteristics and Applications*; Van Nostrand Reinhold: New York, 1991.

(3) Larbot, A.; Fabre, J.-P.; Guizard, C.; Cot, L. *J. Am. Ceram. Soc.* **1989**, *72*, 257.

(4) Hyun, S. H.; Kang, B. S. *J. Am. Ceram. Soc.* **1996**, *79*, 279.

(5) Lin, Y. S.; Burggraaf, A. J. *AIChE J.* **1992**, *38*, 445.

(6) Burggraaf, A. J. Transport and Separation Properties of Membranes with Gases and Vapours. In *Fundamentals of Inorganic Membrane Science and Technology*; Burggraaf, A. J., Cot, L., Eds.; Elsevier: New York, 1996; p 331.

(7) Abeles, B.; Chen, L. F.; Johnson, J. W.; Drake, J. M. *Isr. J. Chem.* **1991**, *31*, 99.

(8) Way, J. D.; Roberts, D. L. *Sep. Sci. Technol.* **1992**, *27*, 29.

(9) Shelekhin, A. B.; Dixon, A. G.; Ma, Y. H. *J. Membr. Sci.* **1992**, *75*, 233.

(10) Delange, R. S. A.; Keizer, K.; Bruggraaf, A. J. *J. Membr. Sci.* **1995**, *104*, 81.

(11) Morooka, S.; Yan, S.; Kusakabe, K.; Akiyama, Y. *J. Membr. Sci.* **1995**, *101*, 89.

(12) Huang, S. C.; Lin, T. F.; Lu, S. Y.; Chou, K. S. *J. Mater. Sci.* **1999**, *34*, 4293.

(13) Nijmeijer, A.; Bladergroen, B. J.; Verweij, H. *Microporous Mesoporous Mater.* **1998**, *25*, 179.

(14) Tsapatsis, M.; Kim, S.; Nam, S. W.; Gavalas, G. *Ind. Eng. Chem. Res.* **1991**, *30*, 2152.

(15) Tsapatsis, M.; Gavalas, G. R. *AIChE J.* **1992**, *38*, 847.

(16) Kim, S.; Gavalas, G. R. *Ind. Eng. Chem. Res.* **1995**, *34*, 168.

(17) Ott, A. W.; McCarley, K. C.; Klaus, J. W.; Way, J. D.; George, S. M. *Appl. Surf. Sci.* **1996**, *107*, 128.

(18) Ott, A. W.; Klaus, J. W.; Johnson, J. M.; George, S. M.; McCarley, K. C.; Way, J. D. *Chem. Mater.* **1997**, *9*, 707.

(19) Berland, B. S.; Gartland, I. P.; Ott, A. W.; George, S. M. *Chem. Mater.* **1998**, *10*, 3941.

(20) Pan, M.; Cooper, C.; Lin, Y. S.; Meng, G. Y. *J. Membr. Sci.* **1999**, *158*, 235.

(21) George, S. M.; Ott, A. W.; Klaus, J. W. *J. Phys. Chem.* **1996**, *100*, 13121.

10.1021/la9916981 CCC: $19.00
Published on Web 06/10/2000

in an ABAB... reaction sequence to deposit Al_2O_3 on alumina membranes.[17−19] In situ N_2 conductance measurements revealed that the pore diameters were reduced from ∼50 Å to molecular diameters at a rate of ∼2.5 Å/AB cycle.[19] In addition, the N_2 conductance was sensitive to the species on the pore surface. $AlCH_3$* species form after $Al(CH_3)_3$ exposures, whereas AlOH* species remain after H_2O exposures. The N_2 conductance indicated that the pore diameters increased by ∼2 Å when AlOH* species replaced $AlCH_3$* species on the pore surface.[19]

In addition to Al_2O_3, other inorganic materials have desirable mechanical, chemical, and thermal properties and can be deposited using ALD methods.[21] The ALD growth technique is based on sequential self-limiting surface reactions and is ideally suited for binary compounds.[21−23] The ALD of various oxides,[24−29] nitrides,[30,31] sulfides,[32] and phosphides[33] has been demonstrated using sequential surface reactions. The ALD of these binary compounds may be useful in reducing the pore diameter of porous membranes and in changing the chemical nature of the membrane.

ALD methods can be employed to deposit both SiO_2[27,28,34] and TiO_2.[24−26] SiO_2 (silica) is an important and widespread inorganic material with high thermal and chemical stability.[1,35] TiO_2 (titania) is also a thermochemically stable inorganic material that displays interesting photocatalytic properties.[1,2,4] SiO_2 and TiO_2 ALD on porous Al_2O_3 tubular membranes should be possible using sequential surface reactions. The surface chemistry of SiO_2 ALD and SiO_2 thin film growth have been described in earlier studies.[27,28,34,36,37] The surface chemistry of TiO_2 ALD and TiO_2 thin film growth have also been the subject of numerous investigations.[24−26,38,39]

For the ALD of SiO_2 films, the $SiCl_4 + 2H_2O \rightarrow SiO_2 + 4HCl$ reaction for SiO_2 chemical vapor deposition (CVD) is divided into the following two half-reactions:[27,28,34,36]

$$\text{(A)} \quad SiOH^* + SiCl_4 \rightarrow SiOSiCl_3^* + HCl \qquad (1)$$

$$\text{(B)} \quad SiCl^* + H_2O \rightarrow SiOH^* + HCl \qquad (2)$$

where the asterisks indicate the surface species. Each reaction is self-limiting and proceeds to completion at sufficient temperatures and reactant exposure.[34] The repetition of these reactions in an ABAB... reaction sequence deposits SiO_2 films on Si(100) with a growth rate of 1.1 Å/AB cycle at 600 K.[27] SiO_2 films can also be grown at room temperature using either pyridine or NH_3 as a Lewis base catalyst.[28,36,37]

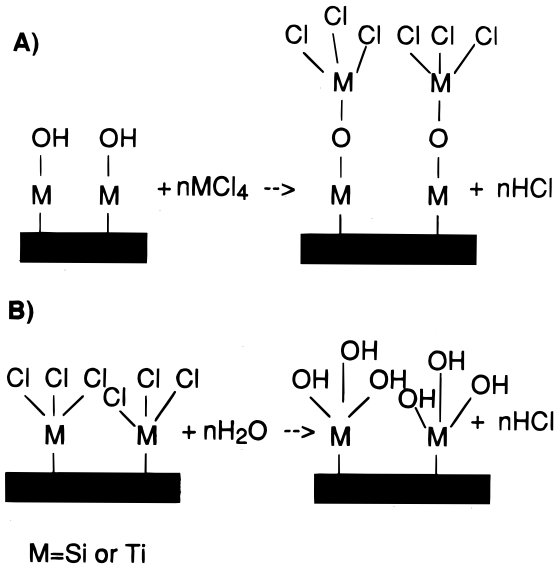

Figure 1. Surface reactions for SiO_2 and TiO_2 atomic layer deposition. M represents either Si or Ti.

For the ALD of TiO_2 films, the $TiCl_4 + 2H_2O \rightarrow TiO_2 + 4HCl$ reaction for TiO_2 CVD is divided into the following two half-reactions:[25,26,38]

$$\text{(A)} \quad TiOH^* + TiCl_4 \rightarrow TiOTiCl_3^* + HCl \qquad (3)$$

$$\text{(B)} \quad TiCl^* + H_2O \rightarrow TiOH^* + HCl \qquad (4)$$

The repetition of these reactions in an ABAB reaction sequence deposits TiO_2 films on flat glass substrates with a growth rate of 0.4−0.6 Å/AB cycle at temperatures from 425 to 800 K.[25,40] Larger TiO_2 growth rates can be observed if insufficient purge times are employed after the $TiCl_4$ and H_2O reactant exposures.[26,40] The growth conditions also affect the structure and morphology of the deposited TiO_2 films.[26,40−42] The surface chemical reactions occurring during SiO_2 and TiO_2 ALD are illustrated in Figure 1.

In this paper, the pore diameters in alumina tubular membranes were progressively reduced using SiO_2 and TiO_2 ALD. In situ N_2 conductance techniques were used to monitor the pore diameter reduction during the alternating exposures to the $SiCl_4/H_2O$ and $TiCl_4/H_2O$ reactants.[19] Progressive pore reduction was observed versus the number of AB cycles. In addition, the N_2 conductance was sensitive to the surface species on the pores during the ABAB... reaction sequence. These results indicate that ALD techniques should be useful in reducing pore diameters and attaching surface functional groups onto pore surfaces for optimized gas separation.

II. Experimental Section

A. Deposition Chamber and Alumina Tubular Membranes. The deposition chamber used to perform the pore reduction experiments has been described earlier.[19] A schematic

(22) Goodman, C. H. L.; Pessa, M. V. *J. Appl. Phys.* **1986**, *60*, R65.
(23) Suntola, T. *Thin Solid Films* **1992**, *216*, 84.
(24) Kumagai, H.; Matsumoto, M.; Toyoda, K.; Obara, M.; Suzuki, M. *Thin Solid Films* **1995**, *263*, 47.
(25) Ritala, M.; Leskela, M.; Nykanen, E.; Soininen, P.; Niinisto, L. *Thin Solid Films* **1993**, *225*, 288.
(26) Aarik, J.; Aidla, A.; Uustare, T.; Sammelselg, V. *J. Cryst. Growth* **1995**, *148*, 268.
(27) Klaus, J. W.; Ott, A. W.; Johnson, J. M.; George, S. M. *Appl. Phys. Lett.* **1997**, *70*, 1092.
(28) Klaus, J. W.; Sneh, O.; George, S. M. *Science* **1997**, *278*, 1934.
(29) Ott, A. W.; Klaus, J. W.; Johnson, J. M.; George, S. M. *Thin Solid Films* **1997**, *292*, 135.
(30) Klaus, J. W.; Ott, A. W.; Dillon, A. C.; George, S. M. *Surf. Sci.* **1998**, *418*, L14.
(31) Morishita, S.; Sugahara, S.; Matsumura, M. *Appl. Surf. Sci.* **1997**, *112*, 198.
(32) Han, M.; Luo, Y.; Moryl, J. E.; Chen, J. G.; Osgood, R. M. *Surf. Sci.* **1998**, *415*, 251.
(33) Ishii, M.; Iwai, S.; Kawata, H.; Ueki, T.; Aoyagi, Y. *J. Cryst. Growth* **1997**, *180*, 15.
(34) Sneh, O.; Wise, M. L.; Ott, A. W.; Okada, L. A.; George, S. M. *Surf. Sci.* **1995**, *334*, 135.
(35) Iler, R. K. *The Chemistry of Silica*; John Wiley and Sons: New York, 1979.
(36) Klaus, J. W.; Sneh, O.; Ott, A. W.; George, S. M. *Surf. Rev. Lett.* **1999**, *6*, 435.
(37) Klaus, J. W.; George, S. M. *Surf. Sci.* **2000**, *447*, 81.
(38) Lakomaa, E.-L.; Haukka, S.; Suntola, T. *Appl. Surf. Sci.* **1992**, *60/61*, 742.
(39) Haukka, S.; Lakomaa, E. L.; Root, A. *J. Phys. Chem.* **1993**, *97*, 5085.
(40) Aarik, J.; Aidla, A.; Sammelself, V.; Uustare, T. *J. Cryst. Growth* **1997**, *181*, 259.
(41) Aarik, J.; Aidla, A.; Sammelselg, V.; Siimon, H.; Uustare, T. *J. Cryst. Growth* **1996**, *169*, 496.
(42) Ritala, M.; Leskela, M.; Johansson, L. S.; Niinisto, L. *Thin Solid Films* **1993**, *228*, 32.

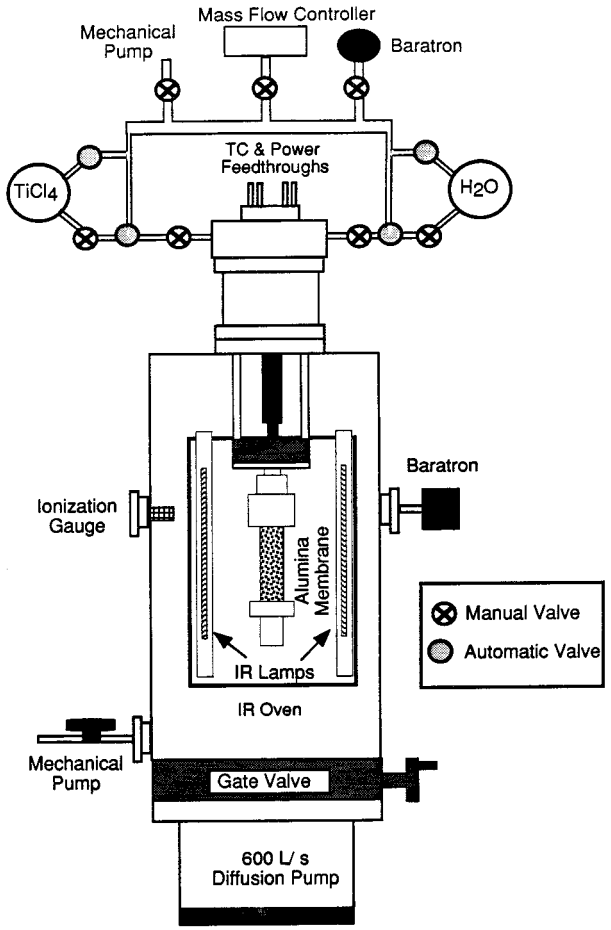

Figure 2. Schematic representation of the deposition chamber utilized to reduce the pore diameter in alumina tubular membranes.

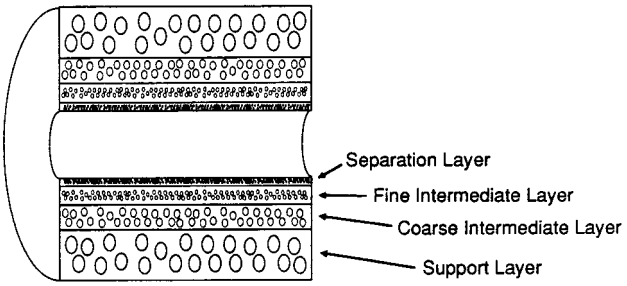

Figure 3. Cross-sectional view of an asymmetric microporous tubular Al_2O_3 membrane from U.S. Filter Ceramic Membrane Products.

of the deposition chamber is shown in Figure 2. The vacuum chamber was pumped by a 600 L/s diffusion pump backed by a mechanical pump. The chamber could also be pumped directly by a rotary vane mechanical pump during high-pressure experiments. The pressure in the chamber was monitored either by a Bayard-Alpert ionization gauge or a 1000 Torr Baratron capacitance manometer.

Asymmetric microporous tubular membranes from U.S. Filter Ceramic Membrane Products (Warrendale, PA) were used for both the SiO_2 and the TiO_2 ALD experiments. A schematic of the cross section of these asymmetric membranes is shown in Figure 3. The tubes were 50 mm long with an inner diameter of 7 mm and an outer diameter of 10 mm. The support layer is composed of α-Al_2O_3 and has a mean pore diameter of 12 μm. The intermediate layers are also composed of α-Al_2O_3. The coarse intermediate layer is a 40 μm thick section and has a mean pore diameter of 0.8 μm. The fine intermediate layer is 20 μm thick and has a mean pore diameter of 0.2 μm. The separation layer is 3−5 μm thick and is composed of γ-Al_2O_3 with a mean pore diameter of 50 Å. The pores in each layer are the voids between the incompletely sintered alumina particles. Consequently, the pores are tortuous with a complex geometry. The effective pore size distribution in the separation layer is narrow with 90% of the pore diameters between 45 and 55 Å.[43]

The ends of the alumina tubular membranes were sealed with a commercial lead−silicate ceramic glaze (Heraeus Cermalloy Division, West Conshohocken, PA). This glaze prevented the gas from entering the end of the membrane by forcing the gas flow inside the tubular membrane. The membrane was mated to the gas lines that deliver the gas reactants using stainless steel Swagelok fittings and graphite ferrules. The opposite end of the membrane was plugged using a Swagelok cap with graphite ferrules.

The Al_2O_3 membranes were heated by an infrared oven surrounding the membrane as shown in Figure 2. The oven consisted of four ~9 in. infrared (IR) lamps mounted inside a cylindrical stainless steel reflector. The IR lamps were positioned evenly around the membrane to ensure uniform heating. Voltage was supplied to the IR lamps using a Variac. The oven temperature could be controlled by manually varying the voltage on the Variac.

The temperature of the alumina tubular membranes could be controlled between 300 and 1000 K. Because of the manual control, the temperature typically varied by as much as ±3−5 K from the desired growth temperature. Type K chromel−alumel thermocouple wires were attached to the membrane and to the stainless steel reflector to monitor the temperature. The reflector also encased the last portion of the reactant gas supply line from the gas manifold. This design allowed the reactant gases to be preheated to the reaction temperature prior to exposure to the porous membrane. Small diameter pores adsorb organic molecules and H_2O over time when left in air. After the alumina tubular membranes were mounted, they were heated to ~750 K for 1−2 h using the IR reflector oven to remove any adsorbed molecules from the pores.[44]

B. SiO_2 and TiO_2 Atomic Layer Deposition. The $SiCl_4$ (silicon tetrachloride, Aldrich), $TiCl_4$ (titanium tetrachloride, Alfa Aesar), and H_2O (distilled and deionized) reactant gases were introduced into the pores of the alumina membrane using a gas manifold. The stainless steel reservoirs of $SiCl_4$ and H_2O were purified with multiple freeze−pump−thaw cycles using liquid nitrogen. $TiCl_4$ was stored in a glass coldfinger and was also purified by freeze−pump−thaw cycles.

SiO_2 (TiO_2) was deposited using alternating exposures of $SiCl_4$ ($TiCl_4$) and H_2O. One AB cycle consisted of a $SiCl_4$ ($TiCl_4$) exposure, a N_2 purge, a H_2O exposure, and a second N_2 purge. The gas source could easily be switched between the reactant exposure and the N_2 purge using automated on−off valves from General Valve.[19] The N_2 gas flow was controlled using a 1−100 standard cubic centimeter per minute (sccm) mass flow controller (MKS, 1159B).

The N_2 purges are required to remove the previous reactant and to avoid chemical vapor deposition. Recent studies of TiO_2 ALD have shown that the N_2 purge time can markedly affect the TiO_2 growth rate per AB cycle.[40] The required reactant exposures and N_2 purge lengths were experimentally determined by monitoring the pore diameter reduction using N_2 conductance measurements. These experimental parameters were obtained using separate alumina tubular membranes.

Previous experiments on flat Si(100) surfaces have demonstrated that $SiCl_4$ and H_2O reactant exposures of 1 Torr for 17 min at 600 K were sufficient for the half-reactions to reach completion during SiO_2 ALD.[27] Larger exposures may be needed for the high-aspect-ratio porous Al_2O_3 membranes. For the reduction of the pore diameters, the initial $SiCl_4$ and H_2O exposures were 20 Torr for 15 min at 600 K. Even larger reactant exposures were required as the conductance decreased with reduced pore diameter.

The following sequence of exposures constituted one AB cycle for SiO_2 at 600 K. First, the Al_2O_3 membrane was exposed to

(43) Sondhi, R. U.S. Filter Ceramic Membrane Products, DeLand, FL. Personal communication, 2000.

(44) Dillon, A. C.; Ott, A. W.; Way, J. D.; George, S. M. *Surf. Sci.* **1995**, *322*, 230.

20 Torr of H_2O for 15 min. The excess H_2O was then removed by pumping on the gas manifold for 5 min and purging with N_2 for 20 min. Subsequently, the alumina membrane was exposed to 20 Torr of $SiCl_4$ for 15 min. The $SiCl_4$ exposure was followed by pumping on the gas manifold for 5 min and then purging with N_2 for 20 min.

The $TiCl_4$ and H_2O reactants for TiO_2 ALD were also exposed to the alumina tubular membrane with N_2 purging between each reactant exposure. One AB cycle of $TiCl_4$ and H_2O at 400 K consisted of a $TiCl_4$ exposure for 25−30 min at 5−12 Torr. The $TiCl_4$ pressure increased as the pore diameters were reduced by TiO_2 deposition. The $TiCl_4$ exposures were followed by a 10−20 min N_2 purge. Subsequently, the tubular membrane was exposed to H_2O for 5 min at 7−15 Torr. The H_2O pressure increased as the pores were reduced by TiO_2 deposition. The H_2O exposure was followed by a ≥30 min N_2 purge.

C. N_2 Conductance Measurements. For in situ monitoring of the pore diameter reduction, N_2 conductance measurements were performed at the reaction temperatures.[19] The conductance of the total system, $C_t = Q/\Delta P_t$, was determined by measuring the total pressure drop, ΔP_t. The N_2 gas throughput, Q, was set at a constant rate between 1 and 10 sccm. At equilibrium, the gas throughput is equal to the gas flow set by the mass flow controller. The pressure was measured in the gas manifold, P_1, and in the vacuum chamber, P_3, using the Baratron pressure gauges. P_2 is the pressure at the downstream end of the gas line immediately adjacent to the membrane.

The total measured conductance, C_t, is a combination of conductance contributions from three sources.[19] One conductance source is the $^1/_8$ in. tubing of the gas line, C_g. The gas flow through the gas line is in viscous flow. The conductance of the gas line is:

$$C_g = 0.0036(P_1 + P_2)/2 \quad (5)$$

where P is given in Torr and C_g in L/s. C_g was measured separately without a tubular membrane mounted in the vacuum chamber. Without a tubular membrane connected to the gas line, $P_2 = P_3 \sim 0$.

The second conductance source is the pores in the alumina tubular membrane, C_p. At all the pressures utilized in these experiments, the gas flow through the pores is in Knudsen flow. An additional flow of N_2 through defects in the membrane and leaks in the membrane mounting seals is in parallel with the flow through the pores. This third conductance source is designated by C_s. Depending on the pressure and size of the defects or sealing leaks, this gas flow is in Knudsen, transition, or viscous flow.[45,46]

The experimental results show that C_t is progressively reduced versus the number of AB cycles and then becomes constant after multiple AB cycles. This behavior argues that the initial 50 Å pores in the alumina tubular membrane are closed after a certain number of AB cycles. In contrast, the multiple AB cycles should negligibly affect the much larger defects or sealing leaks. For most of the experimental pressure range, the pressure drop in the gas line is small enough that the conductance of the transmembrane pressure drop is approximately equal to the total pressure drop, i.e., $C_t \approx C_p + C_s$. Consequently, the constant C_t value obtained after pore closure is attributed to the conductance of gas flow through defects or sealing leaks, C_s.

The combined conductance of the pores and defects or sealing leaks, $C_m = C_p + C_s$, can be separated from the total conductance. The actual pressure drop across the membrane, $\Delta P_m = P_2 - P_3$, must be calculated to accomplish this task. The pressure in the vacuum chamber, P_3, is ~0 Torr. P_2 can be calculated from the pressure drop in the gas line:

$$\Delta P_g = P_1 - P_2 = Q/C_g \quad (6)$$

Substitution of C_g from eq 5 into eq 6 yields an equation that is quadratic in P_2. Consequently, the pressure immediately adjacent to the membrane, P_2, and the transmembrane pressure drop, $\Delta P_m = P_2 - P_3$, can be calculated as a function of the experimental variables Q and P_1.

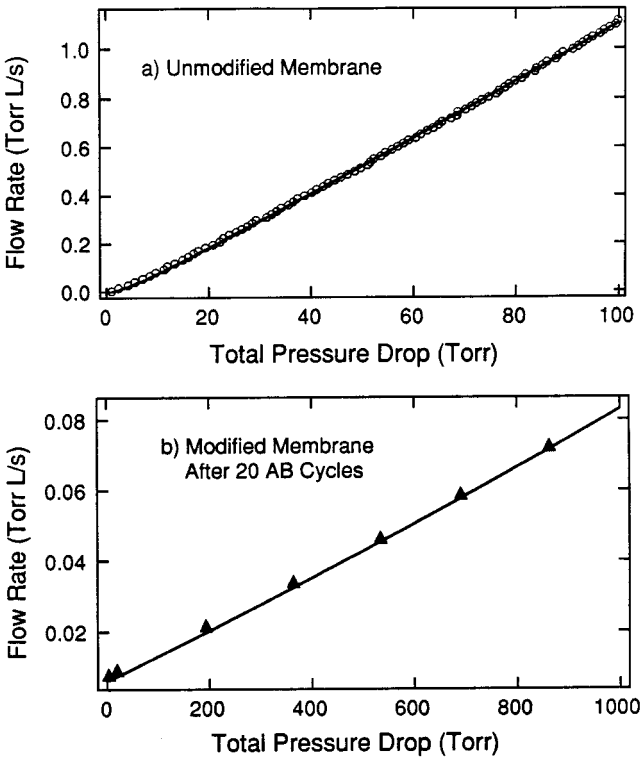

Figure 4. Total pressure drop ($P_1 - P_3$) and N_2 flow rate through (a) an unmodified membrane and (b) the same membrane after 20 AB cycles of TiO_2 deposition.

After the transmembrane pressure drop has been calculated, the combined conductance of the pores and leaks can be determined from $C_m = Q/\Delta P_m = C_p + C_s$. The steady value of C_m after pore closure is assigned to C_s. The value of C_p after each reaction in the ABAB... sequence can then be calculated from $C_p = C_m - C_s$.

The relationship between C_p and D depends on the nature of the pore. If the pores are apertures, then the conductance is dependent on the square of the pore diameter, $C \propto D^2$. The pore diameter can be obtained from C_p according to:[19]

$$D = D_0(C_p/C_0)^{1/2} \quad (7)$$

C_0 designates the initial conductance through the pores, and D_0 is the initial pore diameter. If the pores are cylinders, then the conductance is dependent on the cube of the pore diameter, $C \propto D^3$. The pore diameter is derived from C_p according to:[19]

$$D = D_0(C_p/C_0)^{1/3} \quad (8)$$

The nature of the gas flow through the tubular membrane can be studied by measuring the total pressure drop, P_t, for a series of N_2 flow rates from $Q = 1-90$ sccm. Figure 4a shows a Q versus ΔP_t curve for an unmodified alumina tubular membrane with an initial $C_t = 6.55 \times 10^{-3}$ L/s. Figure 4b displays a Q versus ΔP_t curve for the same membrane with $C_t = 1.10 \times 10^{-4}$ L/s after the pores were closed by 20 AB cycles of TiO_2 deposition. The linear dependence of Q on ΔP_t, observed in Figure 4a, is expected when Knudsen flow through the 50 Å pores dominates C_t. For this tube, the conductance from the defects and sealing leaks was $C_s = 1.10 \times 10^{-4}$ L/s. The initial conductance through the pores was $C_0 = 7.15 \times 10^{-3}$ L/s.

After 20 AB cycles of TiO_2 deposition and pore closure, the Q versus ΔP_t plot also displays a linear dependence as revealed in Figure 4b. This behavior is indicative of Knudsen flow over the full range of pressures. Slight deviations from linearity were observed at higher ΔP values for other tubes. These observations

(45) Roth, A. *Vacuum Technology*; Elsevier Science Publishers: Amsterdam, 1986.

(46) O'Hanlon, J. F. *A User's Guide to Vacuum Technology*; John Wiley & Sons: New York, 1980.

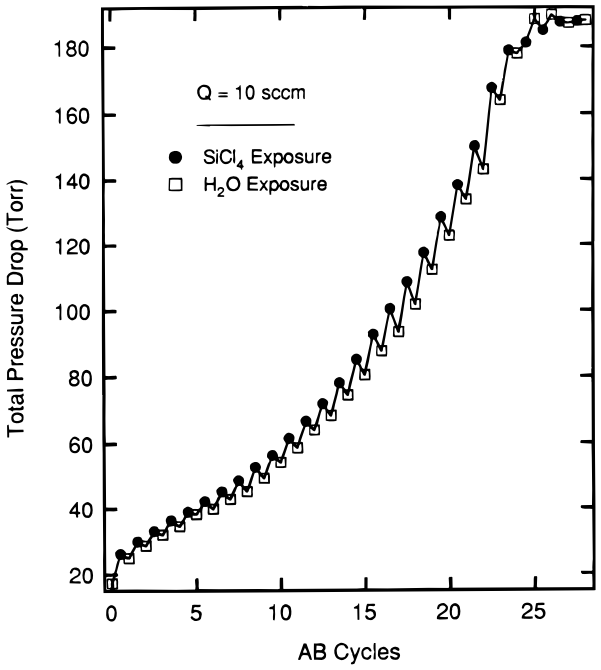

Figure 5. Total pressure drop ($P_1 - P_3$) versus AB cycles at a N_2 flow rate of $Q = 10$ sccm during SiO_2 deposition using alternating $SiCl_4$ and H_2O exposures.

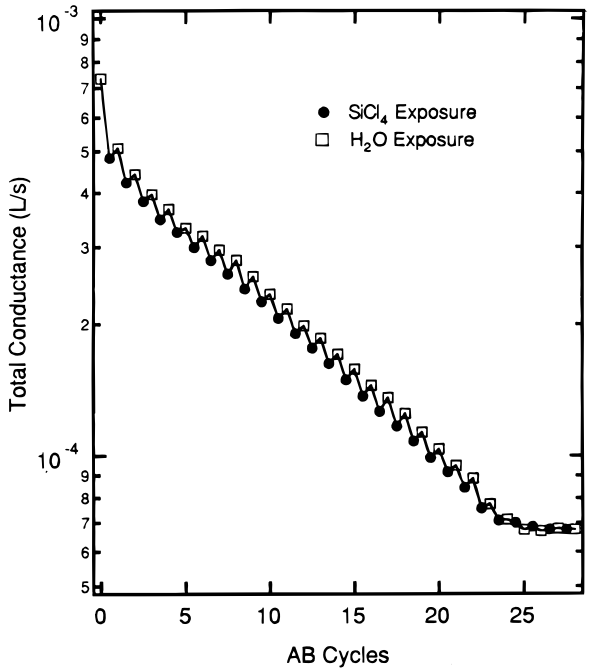

Figure 6. Total N_2 conductance versus AB cycles during SiO_2 deposition. The total pressure drop in Figure 5 was converted to total N_2 conductance by $C_t = Q/\Delta P_t$.

indicate that the gas flow through the defects and sealing leaks is in Knudsen flow at low pressure and transition flow at high pressure.[45,46] This behavior is expected for Knudsen numbers of $n_K > 0.01$. The Knudsen number is defined as $n_K = \lambda/D$, where D is the diameter of the opening and λ is the gas mean free path. Mean free paths at the highest ΔP_t of ~1000 Torr are $\sim 5 \times 10^{-6}$ cm. Consequently, $n_K > 0.01$ is obtained with $D < 5 \times 10^{-4}$ cm. The size of the defects or sealing leaks is expected to be within this limitation.

When the diameter of the gas molecules becomes comparable to the pore diameter at $D < 20$ Å, a transition can occur from Knudsen to configurational diffusion.[47,48] This transition will depend on a number of factors, including the molecular diameter, gas−surface interactions, and the pore diameter.[47] For small and inert molecules such as N_2, this change from Knudsen to configurational diffusion should not occur until pore diameters of 5−10 Å.[47] Consequently, the C_p measurements should be useful in determining pore diameters as small as 5−10 Å assuming Knudsen flow.

III. Results

Figure 5 shows the total pressure drop, ΔP_t, versus the sequential $SiCl_4/H_2O$ AB cycles during SiO_2 ALD at 600 K on an alumina tubular membrane. The N_2 gas flow was fixed at $Q = 10$ sccm. The total pressure drop increases versus AB cycles. In addition, a pronounced oscillation is observed for the total pressure drop between the individual $SiCl_4$ and H_2O exposures. The total pressure drop is consistently higher after the $SiCl_4$ exposures.

Figure 6 shows the conversion of the total pressure drop to total conductance using $C_t = Q/\Delta P_t$. The N_2 conductance versus $SiCl_4/H_2O$ AB cycles drops rapidly after the first $SiCl_4$ exposure. The N_2 conductance then continues to decrease progressively with each AB cycle. The prominent oscillations observed in the total pressure drop after individual $SiCl_4$ and H_2O exposures also appear in the N_2 conductance. The N_2 conductance is consistently smaller after the $SiCl_4$ exposures.

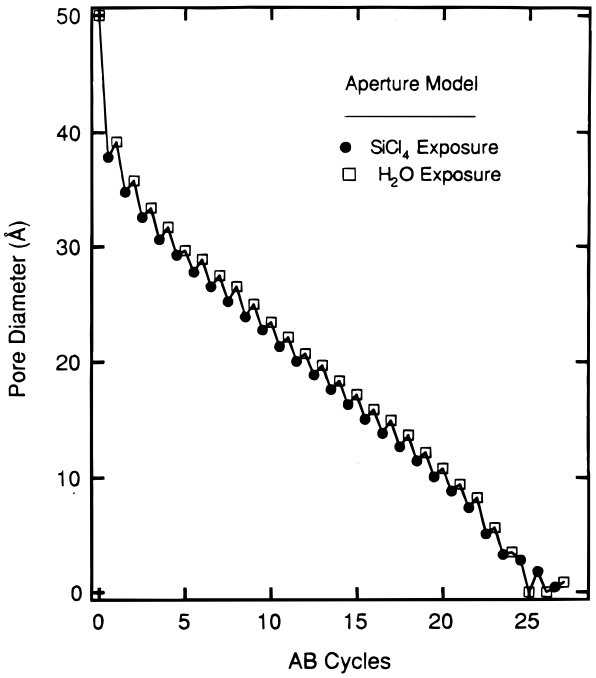

Figure 7. Pore diameter versus AB cycles during SiO_2 deposition. The pore conductance was converted to pore diameter using the aperture model.

The pore diameter was then calculated from $C_p = C_m - C_s$ using the aperture and cylinder pore models. Pore diameters for SiO_2 deposition determined using the aperture model are displayed in Figure 7. Similar results were obtained using the cylinder model. The initial pore diameter of $D_0 = 50$ Å is reduced dramatically to $D = 38$ Å after the first $SiCl_4$ exposure. The pore diameter then decreases linearly with each AB cycle. Pronounced oscillations in the pore diameter are observed after individual $SiCl_4$ and H_2O exposures. The pore diameters are consistently smaller after the $SiCl_4$ exposures.

(47) Xiao, J.; Wei, J. *Chem. Eng. Sci.* **1992**, *47*, 1123.
(48) Shelekhin, A. B.; Dixon, A. G.; Ma, Y. H. *AIChI J.* **1995**, *41*, 58.

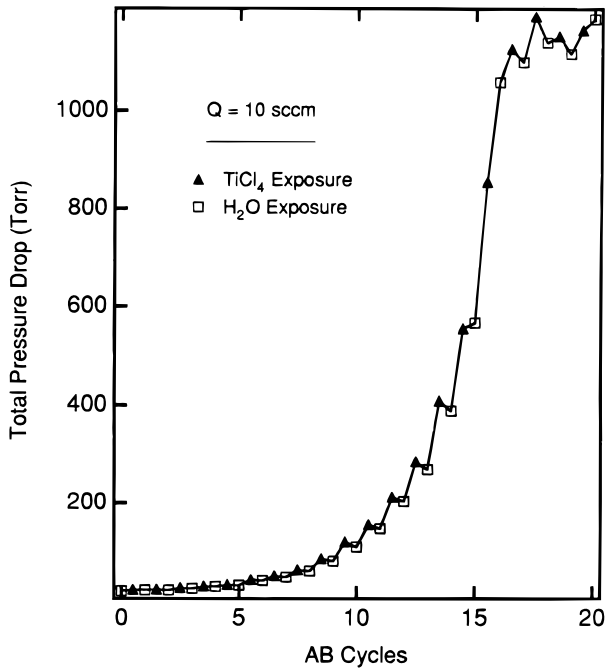

Figure 8. Total pressure drop ($P_1 - P_3$) versus AB cycles at a N_2 flow rate of $Q = 10$ sccm during TiO_2 deposition using alternating $TiCl_4$ and H_2O exposures.

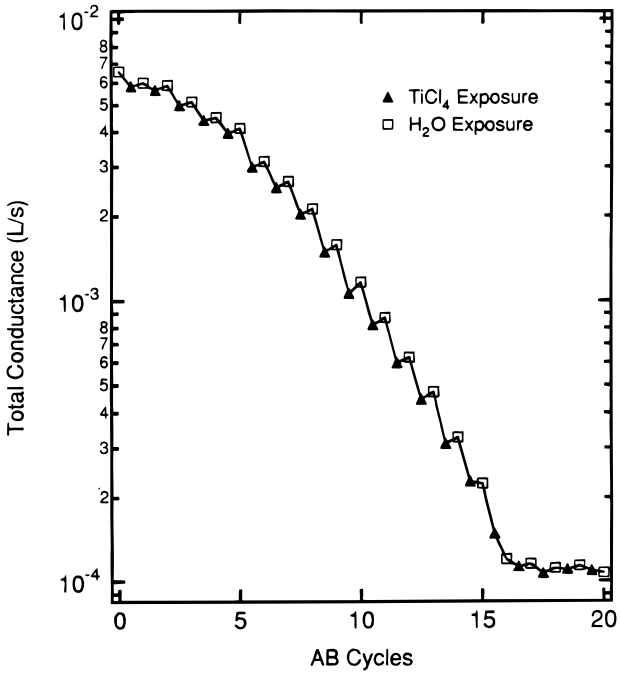

Figure 9. Total N_2 conductance versus AB cycles during TiO_2 deposition. The total pressure drop in Figure 8 was converted to total N_2 conductance by $C_t = Q/\Delta P_t$.

SiO_2 growth rates can be determined from the pore diameter reduction versus AB cycle in Figure 7. The pore diameter decreases at a rate of 1.3 Å ± 0.1 Å per AB cycle according to the aperture model. Consequently, the SiO_2 growth rate on each side of the pore is 0.65 Å/AB cycle. These growth rates are defined in the region where the pore diameter decreases linearly versus AB cycle for AB cycles 6−21. Nearly identical SiO_2 growth rates were derived from the cylinder model. The pores are closed after ~25 AB cycles.

Additional experiments were performed to explore the initial large decrease in pore diameter after the first $SiCl_4$ exposure. In these experiments, the pore diameters were reduced using AB cycles for SiO_2 deposition, followed by AB cycles for Al_2O_3 deposition.[17−19] Subsequently, the pore reduction continued with a few more AB cycles for SiO_2 deposition, followed by a few more AB cycles for Al_2O_3 deposition. The results showed that when the AlOH* species on an Al_2O_3 surface was exposed to $SiCl_4$, a large decrease was always observed in the pore diameter.

Figure 8 shows the total pressure drop, ΔP_t, versus the sequential $TiCl_4/H_2O$ AB cycles during TiO_2 ALD at 400 K on another alumina tubular membrane. The N_2 gas throughput was fixed at $Q = 10$ sccm. The total pressure drop increases versus AB cycles. An oscillation is observed in the total pressure drop after the individual $TiCl_4$ and H_2O exposures. Until the pressure rises rapidly after ~15 AB cycles, the total pressure drop is consistently higher after the $TiCl_4$ exposures.

Figure 9 displays the conversion of the total pressure drop to total conductance using $C_t = Q/\Delta P_t$. The N_2 conductance decreases with each successive $TiCl_4/H_2O$ AB cycle. The oscillations observed in the total pressure drop also appear in the total conductance after individual $TiCl_4$ and H_2O exposures. The N_2 conductance is consistently smaller after the $TiCl_4$ exposures.

The pore diameter was then calculated from $C_p = C_m - C_s$ using the aperture and cylinder pore models. The pore diameters versus AB cycles determined from the aperture model are plotted in Figure 10. Comparable

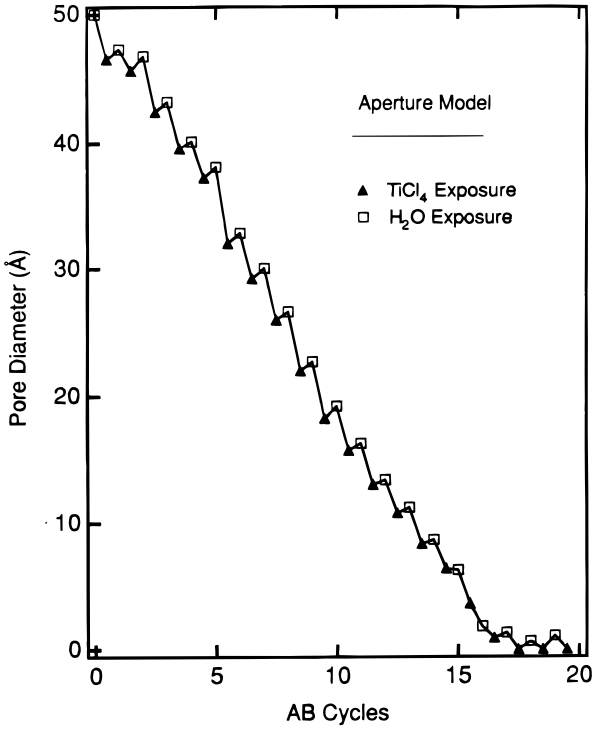

Figure 10. Pore diameter versus AB cycles during TiO_2 deposition. The pore conductance was converted to pore diameter using the aperture model.

results were derived from the cylinder model. The pore diameter is reduced progressively versus AB cycles from the initial pore diameter of $D_0 = 50$ Å. In addition, Figure 10 reveals that oscillations in the pore diameter are observed after individual $TiCl_4$ and H_2O exposures. The pore diameters are consistently smaller after the $TiCl_4$ exposures.

TiO_2 growth rates can be derived from the pore diameter reduction versus AB cycle in Figure 10. The pore diameter decreases at a rate of 3.1 ± 0.9 Å per AB cycle.

Consequently, the TiO_2 growth rate on each side of the pore is 1.55 Å/AB cycle, as determined by the aperture model. These growth rates are defined in the region where the pore diameter decreases linearly versus AB cycle for AB cycles 2−13. Similar TiO_2 growth rates were obtained using the cylinder model. The pores are closed after ∼17 AB cycles.

IV. Discussion

A. Pore Diameter Reduction Rate. The SiO_2 deposition rate of 0.65 Å/AB cycle, obtained from the data in Figure 7, can be compared with the earlier measured SiO_2 deposition rate of 1.1 Å/AB cycle on a flat Si(100) surface at 600 K.[27] The different radii of surface curvatures of the two samples may alter the SiO_2 deposition rate. The porous membrane has an extremely high radius of surface curvature. In contrast, the Si(100) surface is nearly atomically flat and displays a surface roughness of only ±4 Å root mean square (rms). The high radius of curvature of the pore surface may affect the coverage of stable surface species. For example, dehydroxylation via 2SiOH* → Si−O−Si + H_2O may be promoted on the pore surface. The lower stable SiOH* coverage would then lead to less SiO_2 deposited per AB cycle.[27,28,34]

The TiO_2 deposition rate of 1.55 Å/AB cycle obtained from the data in Figure 10 can be compared with an earlier measured TiO_2 deposition rate of 0.4 Å/AB cycle on flat glass substrates at 425 K.[25] Much larger TiO_2 growth rates of ∼1.1 Å/AB cycle were measured on a quartz microbalance at 400−425 K.[26] However, these larger TiO_2 growth rates may be attributed to additional growth from TiO_2 chemical vapor deposition (CVD). TiO_2 CVD may occur if the gas purge times are too short after the $TiCl_4$ and H_2O reactant exposures and if both $TiCl_4$ and H_2O are present in the gas phase.[40] The growth rate of 1.55 Å/AB cycle on the pores of the alumina tubular membrane at 400 K is probably caused by TiO_2 CVD occurring in addition to TiO_2 ALD during each AB cycle. TiO_2 CVD may also explain the larger error bars on the TiO_2 growth rate per AB cycle.

Figure 7 shows that a large reduction in pore diameter is observed after the first $SiCl_4$ exposure during SiO_2 deposition. The aperture model measures a pore diameter reduction of ∼12 Å. This initial reduction is significantly larger than any of the subsequent reductions observed after $SiCl_4$ exposures. In contrast, Figure 10 reveals that the initial pore diameter reduction after the first $TiCl_4$ exposure during TiO_2 deposition is comparable to the reductions observed after subsequent $TiCl_4$ exposures.

The large initial decrease in pore diameter after the first $SiCl_4$ exposure and lower decrease in pore diameter after subsequent $SiCl_4$ exposures may be partially explained by the different hydroxyl coverages on Al_2O_3 and SiO_2 surfaces. Previous studies have determined that SiO_2 has a hydroxyl coverage of ∼3 OH/nm^2 at 600 K.[35,49] In comparison, other investigations have reported that Al_2O_3 has a hydroxyl coverage of ∼6.5 OH/nm^2 at 600 K.[50] Consequently, the initial $SiCl_4$ exposure can react with more hydroxyl groups on the initial Al_2O_3 surface. Fewer hydroxyl groups on the SiO_2 surface will lead to a lower SiO_2 deposition rate after the Al_2O_3 surface is converted to a SiO_2 surface.

Hydrogen magic angle spinning nuclear magnetic resonance (MAS NMR) studies have also recently measured the number of hydroxyl groups on SiO_2 and Al_2O_3 powders after their annealing at 773−823 K.[51] SiO_2 had a measured SiOH* coverage of ∼1.8 OH/nm^2, and Al_2O_3 displayed a AlOH* coverage of ∼3.0 OH/nm^2. Although the annealing temperature of 773−823 K is considerably higher than the SiO_2 growth temperature of 600 K, these MAS NMR investigations confirm the larger number of hydroxyl groups on the Al_2O_3 surface. These MAS NMR studies are consistent with the earlier hydroxyl coverage measurements because the thermal stability of hydroxyl groups on both SiO_2 and Al_2O_3 decreases nearly linearly with temperature from 300 to 1000 K.[34,35,44,50,52]

The hydrogen MAS NMR studies also monitored the conversion of the Al_2O_3 surface to a SiO_2 surface using the sequential exposure to hexamethyldisilazane (HMDS) and air at 773−823 K.[51] The SiO_2 deposition strategy was very similar to the alternating exposures of $SiCl_4$ and H_2O at 600 K employed in the current study. The hydrogen MAS NMR results displayed a pronounced drop in the total hydroxyl coverage from ∼3.0 OH/nm^2 on Al_2O_3 to ∼1.7 OH/nm^2 on Al_2O_3 coated by one HMDS/air reaction cycle.[51] A similarly large decrease in hydroxyl coverage after the first $SiCl_4/H_2O$ cycle could explain the smaller decrease in pore diameter after the first $SiCl_4$ exposure in Figure 7.

Figure 10 shows that the reduction in pore diameter after the first $TiCl_4$ exposure is comparable to the pore diameter reductions after subsequent $TiCl_4$ exposures during TiO_2 deposition. The agreement between these pore diameter reductions may be related to the similar hydroxyl coverages on the Al_2O_3 and TiO_2 surfaces. Several studies have reported the temperature-dependent hydroxyl coverage on the TiO_2 surface.[53,54] At the TiO_2 deposition temperature of 400 K, the hydroxyl coverage on TiO_2 is 9 OH/nm^2,[53] compared with a hydroxyl coverage of 11 OH/nm^2 on Al_2O_3.[50]

B. Minimum Pore Diameter. The determination of the pore diameter is dependent on the conversion of the transmembrane pressure drop to conductance via $C_m = Q/\Delta P_m$. Once C_s is determined after pore closure, $C_p = C_m - C_s$, and the pore diameters can be ascertained using the aperture or cylinder models. These pore diameters are dependent on the assumption that the pores will be completely closed after multiple AB cycles. The accuracy of this assumption will affect the determination of growth rates per AB cycle and the pore diameter differences following the $SiCl_4$, $TiCl_4$, and H_2O reactant exposures.

Our earlier investigation of pore diameter reduction in alumina tubular membranes using alternating Al(CH_3) and H_2O exposures did not assume that the pore diameters were completely closed after a certain number of AB cycles.[19] This study assumed that the C_p and C_s conductance contributions could be determined independently.[19] C_p was believed to be distinguishable from C_s because Knudsen flow through the pores should yield a gas throughput that varies linearly with ΔP. In contrast, the gas flow through the membrane defects and sealing leaks that defines C_s was thought to occur only as viscous flow. This gas throughput should have varied quadratically with ΔP.

Figure 4 shows the Q versus ΔP_t plots and corresponding fits for an alumina tubular membrane before and after TiO_2 deposition. The Q versus ΔP_t plot in Figure 4a displays a linear dependence, as expected for Knudsen flow through the initial 50 Å diameter pores. However,

(49) Sneh, O.; George, S. M. *J. Phys. Chem.* **1995**, *99*, 4639.
(50) Knozinger, H.; Ratnasamy, P. *Catal. Rev. Sci. Eng.* **1978**, *17*, 31.
(51) Lindblad, M.; Root, A. *Prepr. Catal VII* **1998**, *118*, 817.
(52) Peri, J. B.; *J. Phys. Chem.* **1965**, *69*, 211.
(53) Lusvardi, V. S.; Barteau, M. A. *J. Phys. Chem.* **1996**, *100*, 18183.
(54) Suda, Y.; Morimoto, T.; Nagao, M. *Langmuir* **1987**, *3*, 99.

the Q versus ΔP_t plot after 20 AB cycles shown in Figure 4b also reveals an approximately linear dependence. These observations are different than the results from our earlier study of Al_2O_3 deposition in the alumina tubular membranes.[19] After multiple AB cycles when there was no additional change in the total conductance during Al_2O_3 deposition, our earlier study of pore diameter reduction observed a quadratic dependence between Q and ΔP_t.[19] The linear and quadratic dependencies in this earlier Q and ΔP_t plot were deconvoluted to obtain C_p and C_s. In contrast, the lack of quadratic dependence between Q and ΔP_t in the current study has forced us to reevaluate our previous analysis procedure.

We now believe that there may be pressure regimes and defect and sealing leak diameters that can produce a linear dependence between Q and ΔP_t at low pressures and nonlinear dependence at high pressures. The linear dependence will occur for molecular flow in the Knudsen regime when the Knudsen number is >1.[45,46] A change from linear to quadratic dependence will occur in the transition region between molecular flow and viscous flow when $1 > K_n > 0.01$.[46] A linear dependence may also be observed in critical flow through a constriction when $K_n < 0.01$ and the upstream pressure is greater than twice the downstream pressure.[46] Consequently, the linear dependence between Q and ΔP_t cannot be assigned unambiguously to only Knudsen flow through the pores in the tubular membrane.

A more reasonable assumption is that the pores are completely closed after a certain number of AB cycles. The uncertainty of this assumption is affected by the size of the reactants. As the pore diameter approaches the molecular diameter of the reactants, the pores may block the transport of reactants through the membrane. As a result, the pore diameters may reach a minimum pore diameter that is defined by the molecular diameter of the reactants or the molecular diameter of the N_2 gas molecule used to measure the membrane conductance.

The molecular diameters for the $SiCl_4$, $TiCl_4$, and H_2O reactants and the N_2 conductance probe can be obtained from the literature or calculated from physical parameters. For $SiCl_4$, a molecular diameter of $\sim$6.2 Å is calculated using a Si−Cl bond length of 2.02 Å[55] and a chlorine van der Waals radius of 1.77 Å.[56] Likewise, a molecular diameter of $\sim$6.4 Å can be determined for $TiCl_4$, based on the Ti−Cl bond length of 2.2 Å[57,58] and a chlorine van der Waals radius of 1.77 Å.[56] An H_2O molecular volume of 16.82 Å^3 [56] yields an H_2O molecular diameter of $\sim$3.2 Å. The N_2 conductance probe has a molecular diameter of 3.64 Å.[59] These molecular diameters indicate that the minimum pore diameter may be as large as $\sim$6 Å for both SiO_2 and TiO_2 deposition.

Even if the pore diameter is larger than the molecular diameter of the reactants, interactions between the reactants and the pore walls may discourage reaction and deposition. One such possible interaction is "molecular levitation" that can occur when the molecular diameter is slightly less than the pore diameter.[60,61] In this case, the molecule is completely encircled by the pore surface. Physisorption interactions occur through a complete range of angles. This equal attraction over a full 360° leaves the molecule suspended or "levitated" within the pore.[60,61] In this configuration, the molecule may not be able to react with functional groups on the pore surface.

SiO_2 and TiO_2 deposition in the pores may also be reduced or stopped because of a change in coverage of surface species as the pore approaches molecular diameters. The −OH and −Cl species stabilities may be reduced as the radius of curvature is progressively decreased at smaller pore diameters. SiO_2 deposition rates are believed to be directly related to the SiOH surface coverage.[27,28,34,36] If the hydroxyl coverage on the pore surface is lowered as the pore diameter is reduced, then the SiO_2 and TiO_2 growth rates may become negligible at some small pore diameter.

C. Effect of Surface Species on Gas Transport. There is a pronounced oscillation in the total pressure drop, total N_2 conductance, and pore diameter versus $SiCl_4$ and H_2O exposures during SiO_2 deposition and versus $TiCl_4$ and H_2O exposures during TiO_2 deposition. This behavior indicates that surface species have a distinctive effect on N_2 gas flow through membranes when the pore diameters approach molecular diameters. A similar oscillation was observed during Al_2O_3 deposition on Al_2O_3 tubular membranes using alternating $Al(CH_3)_3$ and H_2O exposures.[19] The total pressure drop increases, the total N_2 conductance decreases, and the pore diameter decreases after the $SiCl_4$ and $TiCl_4$ exposures. These exposures deposit Si or Ti on the surface by reaction with surface hydroxyl groups, viz. $MOH^* + MCl_4 \rightarrow MOMCl_3^* + HCl$, where M = Si or Ti. Subsequently, the total pressure drop decreases, the total N_2 conductance increases, and the pore diameter increases after the H_2O exposure that replaces Cl* with OH* on the surface by an exchange reaction, viz., $MCl^* + H_2O \rightarrow MOH^* + HCl$.

According to the aperture model, the pore diameters decrease by 2.2 Å after $SiCl_4$ exposures and 3.8 Å after $TiCl_4$ exposures. This large decrease is expected because the MCl_3* surface species is replacing the H* surface species. After H_2O exposure, the pore diameter increased 0.9 Å during SiO_2 deposition and 0.7 Å during TiO_2 deposition. When initially observed during our Al_2O_3 deposition studies,[19] this increase in pore diameter after H_2O exposures was very surprising. These current SiO_2 and TiO_2 deposition studies were conducted, in part, to determine if this increase was a general effect and if surface species have a dramatic effect on gas transport when pore diameters become comparable to molecular diameters.

The decrease in pore diameter following the $Al(CH_3)$ exposure and the increase in pore diameter following the H_2O exposure during Al_2O_3 deposition was interpreted assuming steric interactions.[19] The effect of steric interactions on the pore diameter is shown in Figure 11. Simple steric interactions predict a large decrease in pore diameter when $SiCl_4$ or $TiCl_4$ reacts with the hydroxyl groups and MCl_3 species are added to the pore surface. Subsequently, the pore diameter increases after the replacement of a Cl* surface species by an OH* surface species.

The expected decrease in pore diameter after $SiCl_4$ and $TiCl_4$ exposures and the increase in pore diameter after H_2O exposure can be calculated assuming steric interactions. These predictions require bond lengths for the Si−O, Ti−O, Si−Cl, and Ti−Cl bonds. In addition, van der Waals radii are needed for the Cl* and OH* surface species. A summary of these bond lengths and van der Waals radii is given in Table 1. Disregarding any angular

(55) *Encyclopedia of Inorganic Chemistry*; King, R. B., Ed.; John Wiley and Sons: New York, 1994; Vol. 7.
(56) Gavezzotti, A.; *J. Am. Chem. Soc.* **1983**, *105*, 5220.
(57) Branchadell, V.; Oliva, A. *J. Am. Chem. Soc.* **1992**, *114*, 4357.
(58) Stashans, A.; Lunell, S.; Grimes, R. W. *J. Phys. Chem. Solids* **1996**, *57*, 1293.
(59) Chen, N. Y.; Degnan, T. F.; Smith, C. M. *Molecular Transport and Reaction in Zeolites: Design and Application of Shape Selective Catalysts*; John Wiley & Sons: New York, 1994.
(60) Derouane, E. G.; Andre, J. M.; Lucas, A. A. *Chem. Phys. Lett.* **1987**, *137*, 336.
(61) Derouane, E. G.; Andre, J. M.; Lucas, A. A. *J. Catal.* **1988**, *110*, 58.

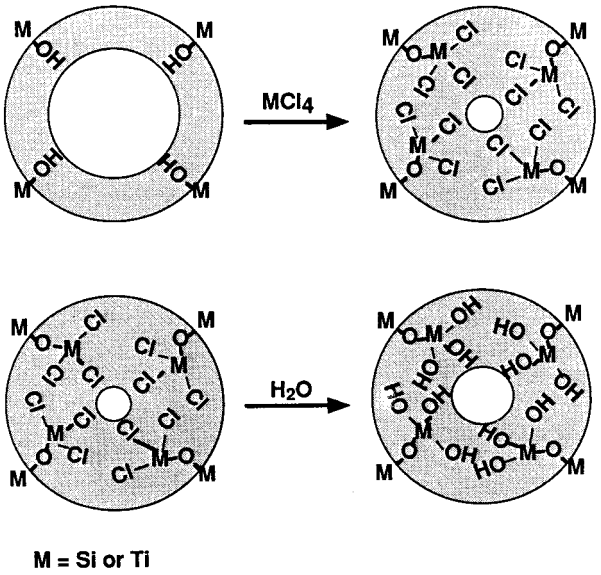

Figure 11. Illustration of the changes in pore diameter after the MCl_4 and H_2O alternating exposures during SiO_2 or TiO_2 deposition. M represents either Si or Ti.

Table 1. Parameters Used To Calculate the Size of the MCl* and MOH* Surface Species after $SiCl_4/TiCl_4$ and H_2O Exposures during SiO_2/TiO_2 Deposition[a]

	Si−Cl	Si−OH	Ti−Cl	Ti−OH
bond length (Å)	2.04 [62]	1.70 [62]	2.2 [57]	1.90 [63]
van der Waals radius (Å)	1.77 [56]	1.45 [56]	1.77 [56]	1.45 [56]
effective diameter (Å)	3.81	3.15	3.97	3.35

[a] Bond lengths and van der Waals radii obtained from references given in brackets.

alignment of the surface species, we can determine the effective diameters of the OH* and Cl* surface species by adding the bond lengths and van der Waals radii (Table 1).[56,57,62,63] These effective diameters are referenced from the position of the underlying Si or Ti atom.

The diameter difference for pores covered with either Cl* or OH* surface species can be determined from the effective diameters in Table 1. During SiO_2 deposition, the pores are predicted to be 1.32 Å larger in diameter after the H_2O exposures. This prediction can be compared with the measurements revealing that the pore diameters are 0.9 ± 0.2 Å larger after the H_2O exposures. During TiO_2 deposition, the pores are predicted to be 1.24 Å larger in diameter after the H_2O exposure. This prediction can be compared with the measurements showing that the pore diameters are 0.7 ± 0.2 Å larger after the H_2O exposures. Although the measured differences are smaller than the predictions assuming steric interactions, the measurements and predictions both indicate that the pore diameters are consistently larger after the H_2O exposures.

Dehydration may also explain the larger pore diameters observed after H_2O exposures. According to eqs 2 and 4, each MCl* species is replaced by MOH* during the H_2O half-reaction. These MOH* species may then undergo dehydroxylation via $2MOH^* \rightarrow MOM^* + H_2O$. The MOH* species are probably pointed toward the center of the pore. On the other hand, the MOM* species resulting from dehydration will have a M−O−M bridge bond that is expected to be aligned more along the circumference of the pore. Consequently, the loss of the MOH* species would increase the pore diameter.

The predictions given in Table 1 assume that only steric interactions determine N_2 transport through the alumina tubular membranes. However, different chemical interactions between N_2 and Cl* and OH* surface species may also alter the N_2 gas transport rate. The earlier investigations of Al_2O_3 deposition using alternating exposures of $Al(CH_3)_3$ and H_2O employed both N_2 and Ar conductance measurements.[19] The oscillations during the $Al(CH_3)_3$ and H_2O alternating exposures were observed for both N_2 and Ar.[19] These results argued that chemical interactions were not significant for the transport of N_2 gas. The similarity of the results versus the alternating $Al(CH_3)_3/H_2O$, $SiCl_4/H_2O$, and $TiCl_4/H_2O$ exposures during Al_2O_3, SiO_2, and TiO_2 deposition, respectively, argues that steric interactions play a major role in determining N_2 gas transport through the porous membranes.

V. Conclusions

Sequential surface reactions were employed to reduce the pore diameters in alumina tubular membranes. The atomic layer deposition (ALD) of SiO_2 and TiO_2 was performed using self-limiting surface reactions. The SiO_2 ALD was achieved using alternating exposures of $SiCl_4$ and H_2O. The TiO_2 ALD was accomplished using alternating exposures of $TiCl_4$ and H_2O. The reduction of the pore diameter was observed using in situ N_2 conductance measurements during the alternating exposures. The total N_2 conductance, $C_t = Q/\Delta P_t$, was measured using a mass flow controller to define a constant gas throughput, Q, and two capacitance manometers to monitor the total pressure drop, ΔP_t.

The N_2 conductance measurements revealed that SiO_2 and TiO_2 ALD progressively reduced the pore diameter of alumina tubular membranes. Using an aperture model to interpret the conductance results, the pore diameter was reduced 1.3 ± 0.1 Å per $SiCl_4/H_2O$ AB cycle during SiO_2 deposition and 3.1 ± 0.9 Å per $TiCl_4/H_2O$ AB cycle during TiO_2 deposition. The N_2 conductance measurements were also very sensitive to the surface species on the pore surface. The pore diameters were 0.9 ± 0.2 Å larger after the H_2O exposure converted the SiCl* species to SiOH* species during SiO_2 deposition. The pore diameters were 0.7 ± 0.2 Å larger after the H_2O exposure converted the TiCl* species to TiOH* species during TiO_2 deposition. These differences were smaller than the differences expected assuming steric interactions between the N_2 gas molecule and the surface species.

Together with the earlier results for Al_2O_3 deposition in alumina tubular membranes using alternating exposures of $Al(CH_3)_3$ and H_2O, these results illustrate that pore diameters can be reduced with atomic layer control using sequential self-limiting surface reactions. The N_2 conductance measurements reveal that gas transport through microscopic pores is determined by pore diameters and the effect of the surface functional groups. For less inert gases, chemical interactions may also play an important role in defining gas transport rates. Tuning the pore diameter and chemical interactions with the surface species may lead to optimized gas separation membranes.

Acknowledgment. This work was funded in part by the Center for Membrane Applied Science and Technology (MAST) at the University of Colorado. This center is

(62) Jenichen, A.; *Int. J. Quantum Chem.* **1994**, *52*, 117.
(63) Lindan, P. J. D.; Harrison, N. M.; Holender, J. M.; Gillan, M. J. *Chem. Phys. Lett.* **1996**, *261*, 246.

sponsored by the National Science Foundation and the Colorado Advanced Technology Institute (CATI). Additional support was provided by the Air Force Office of Scientific Research. The authors thank Brian S. Berland of ITN Energy Systems, Inc., for many useful conversations. We also thank Ken McCarley and Doug Way in the Department of Chemical Engineering and Petroleum Refining at the Colorado School of Mines for helping to prepare the alumina tubular membranes for this study.

LA9916981